

VYSOKÉ UČENÍ TECHNICKÉ V BRNĚ  
BRNO UNIVERSITY OF TECHNOLOGY



FAKULTA STROJNÍHO INŽENÝRSTVÍ  
ÚSTAV FYZIKÁLNÍHO INŽENÝRSTVÍ

FACULTY OF MECHANICAL ENGINEERING  
INSTITUTE OF PHYSICAL ENGINEERING

## RŮSTOVÉ DEFEKTY V MONOKRYSTALECH CZOCHRALSKIHO KŘEMÍKU MICRODEFECTS IN CZOCHRALSKI SILICON

ZKRÁCENÁ VERZE DISERTAČNÍ PRÁCE  
SHORT VERSION OF DOCTORAL THESIS

AUTOR PRÁCE  
AUTHOR

Ing. LUKÁŠ VÁLEK

VEDOUCÍ PRÁCE  
SUPERVISOR

prof. RNDr. JIŘÍ SPOUSTA, Ph.D.

STŘÍTEŽ NAD BEČVOU 2012

**Klíčová slova**

Křemík, Czochralski, bór, defekty, vrstevné chyby, precipitace kyslíku

**Keywords**

Czochralski silicon, boron, microdefects, oxidation induced stacking faults, oxygen precipitation

# **OBSAH**

1	MOTIVATION.....	4
2	GOALS .....	4
3	STUDY OF CRYSTAL DEFECTS IN HEAVILY BORON-DOPED SILICON .	5
3.1	EXPERIMENTAL .....	5
3.2	OISF ON HEAVILY BORON-DOPED WAFERS.....	6
3.3	DEPENDENCE OF OISF DISTRIBUTION ON DOPING LEVEL AND POSITION IN THE CRYSTAL .....	6
3.4	SIMULATION OF THE V-I BOUNDARY .....	7
3.5	ESTIMATION OF THE CRITICAL VALUE $V/G$ .....	8
3.6	COMPARISON OF V-I BOUNDARY SIMULATIONS WITH OISF DISTRIBUTION .....	10
3.7	RADIAL OISF DISTRIBUTION .....	11
3.8	RELATION OF OISF TO BULK CRYSTAL DEFECTS .....	12
3.9	ORIGIN OF THE RADIAL OISF PATTERN .....	13
3.10	VERIFICATION OF THE V-I BOUNDARY.....	15
3.11	ORIGIN OF THE AXIAL CHANGES IN THE OISF PATTERN.....	15
3.12	OISF TEST WITH PRE-ANNEALING.....	17
3.13	ORIGIN OF THE AXIAL VARIATIONS IN THE SIZE OF GROWN-IN OXIDE PRECIPITATES .....	19
3.14	SUMMARY ON FORMATION OF THE OISF PATTERN .....	21
3.15	ENHANCED PRECIPITATION OF OXYGEN.....	22
3.16	INFLUENCE OF BORON ON OXYGEN PRECIPITATION .....	23
4	SUMMARY.....	25
	LITERATURA .....	27
	CURRICULUM VITAE.....	29
	ABSTRAKT .....	30
	ABSTRACT .....	30

# 1 MOTIVATION

ON Semiconductor is a worldwide producer of silicon-based discrete devices and integrated circuits for electronics. ON Semiconductor Czech Republic (CR) supplies the corporation with starting material — silicon wafers — manufactured from the silicon single crystals grown by the Czochralski method. Various defects are formed in the lattice of the growing crystal, which can influence the performance and reliability of devices made on the silicon wafers. This work is focused on study of the crystal defects in silicon and implementation and development of tools for their control.

As a particular example, it was found that Zener diodes manufactured on silicon wafers heavily doped with boron suffer from severe leakage current. Further analyses revealed the correlation of the leakage currents to the presence of crystal defects in the wafers. Due to scrapping of the afflicted wafers, the company encounters financial loss. Hence, there is a need for control of wafer quality from the defect point of view.

# 2 GOALS

The goals of the work are:

- analyses of microdefects in silicon crystals;
- computer simulations of Czochralski silicon crystal growth;
- computer simulations of defect distribution in the crystals;
- explanation of observed microdefect distribution and construction of a model of defect formation;
- study of possibilities of defect control.

### 3 STUDY OF CRYSTAL DEFECTS IN HEAVILY BORON-DOPED SILICON

Specifications of some types of polished silicon wafers include a requirement for maximal allowed surface density of OISF (Oxidation Induced Stacking Faults). In such case, monitoring wafers are sampled from the whole crystal. These wafers pass OISF test and OISF density is checked. The 150 mm heavily boron-doped wafers produced in ON Semiconductor CR are the typical representatives of products with such specifications. Heavy doping corresponds roughly to the level of above  $10^{17} \text{ cm}^{-3}$  atoms of boron in silicon.

Evaluation of OISFs on these products revealed unacceptably high OISF density in the seed-end portion of the crystals. These crystal portions cannot be used for production of silicon wafers with specified OISF density. In case this material fulfills specification of other required product, it is utilized for its manufacturing; otherwise it is scrapped. The resulting financial and capacity losses drove the requirement to solve the problem. In order to control the OISF density effectively one has to understand the mechanisms of their formation.

#### 3.1 EXPERIMENTAL

Single crystals of silicon of 6" diameter, (111) oriented, boron-doped were grown by the Czochralski method in ON Semiconductor CR from a standard 16" hot zone and 35 kg polysilicon charge. The cylindrical part of the crystal of total length of about 620 mm was cut into several peaces (usually 3–4). Thick wafers (2–3 mm), so called slugs, were sliced from the faces of the crystal parts for measurement of oxygen concentration and resistivity. Resistivity was measured by the four-point-probe and the measured values were converted into volume concentration of boron in silicon according to the ASTM standard [1]. Oxygen concentration in heavily doped crystals was measured by secondary ion mass spectroscopy (SIMS). Fourier transform infrared spectroscopy (FTIR) was used to measure oxygen concentration in lightly doped crystals grown by the same process as the heavily doped crystals (recipe, hot zone). Oxygen concentration in the heavily doped crystals was assumed to be the same as in the lightly doped ones (this was verified earlier on different boron-doped products). The conversion factor of  $4.815 \times 10^{17} \text{ cm}^{-2}$  after ASTM 1979 [2] was used ("old ASTM"). Boron concentration in the studied crystals was  $9 \times 10^{14} - 5 \times 10^{19} \text{ cm}^{-3}$  (resistivity 15–0.002  $\Omega\text{cm}$ ); oxygen concentration was in the range of 25–35 ppma. The crystals were processed into single-side polished silicon wafers of diameter of 150 mm and thickness of 625  $\mu\text{m}$ .

Crystal defects in the wafers were analyzed by OISF test, COP test and X-ray section topography. OISF test was performed by oxidation of polished wafers in wet atmosphere at 1150°C for 3 h. Silicon oxide grown during the OISF test was stripped by hydrofluoric acid (42%, 5 min) and the wafer was selectively etched by Yang etchant [3] for 1 min. Part of the wafers was annealed prior to the OISF test in a non-oxidizing ambient ( $\text{N}_2:\text{O}_2$  in ratio 20:1) at 1050°C for 10 h. OISF

distribution across the wafer surface was observed by naked eye under collimated light and by optical microscope. Radial profile of the OISF surface density was constructed by counting of OISFs along wafer diameter in two perpendicular directions; OISF density was averaged from these two measurements. The COP test was performed by wafer etching in SC1 solution ( $\text{NH}_4\text{OH}:\text{H}_2\text{O}_2:\text{H}_2\text{O}$  in ratio 1:1:5) at 70–80°C for 4 h. The COP distribution was analyzed using the particle counter KLA Tencor Sufscan 6220. The X-ray section topographs were taken with JEOL JMX-8H micro-focus X-ray diffractometer in Laue geometry using  $\text{Ag K}_{\alpha 1}$  radiation and  $\langle 440 \rangle$  diffraction. Bulk defects were observed on digitalized pictures.

### 3.2 OISF ON HEAVILY BORON-DOPED WAFERS

The status of the problem at the beginning of my work was as follows. The seed-end portions of the heavily boron-doped crystals could not be utilized for manufacturing of polished wafers because of the very high counts of OISFs. This portion was the first 150 mm out of total 600 mm of the crystal length. The rest of the crystal was sampled and OISF density was checked to verify that the OISF specification is met. Some of the tested wafers were completely OISF-free; some contained certain amount of OISFs. Circular pattern of OISFs could be recognized on some of the wafers. The pattern was either a circle or a circle with an extra outer ring (Fig. 1). It was believed that the OISF patterns have some relation to the OISF ring described in the literature but their origin remained unclear due to a different shape compared to the OISF ring.

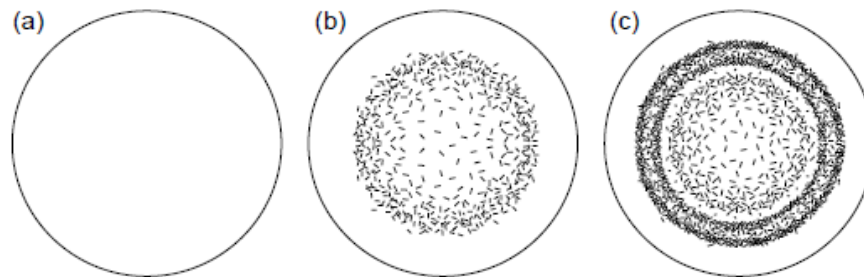


Figure 1: OISF distribution observed on the surface of 150 mm heavily boron-doped silicon wafers. (a) Clean wafer, (b) circular OISF pattern, (c) circular OISF pattern with an extra outer ring.

### 3.3 DEPENDENCE OF OISF DISTRIBUTION ON DOPING LEVEL AND POSITION IN THE CRYSTAL

Fig. 2 shows the measured radii of the observed OISF pattern after exclusion of the outlayers. The resistivity was found out for each data point to distinguish the effect of boron doping. The apparent dependence of the OISF pattern radius on the resistivity is revealed as well as dependence of the OISF pattern radius on the position in the crystal. The radial distribution of OISF and its dependence

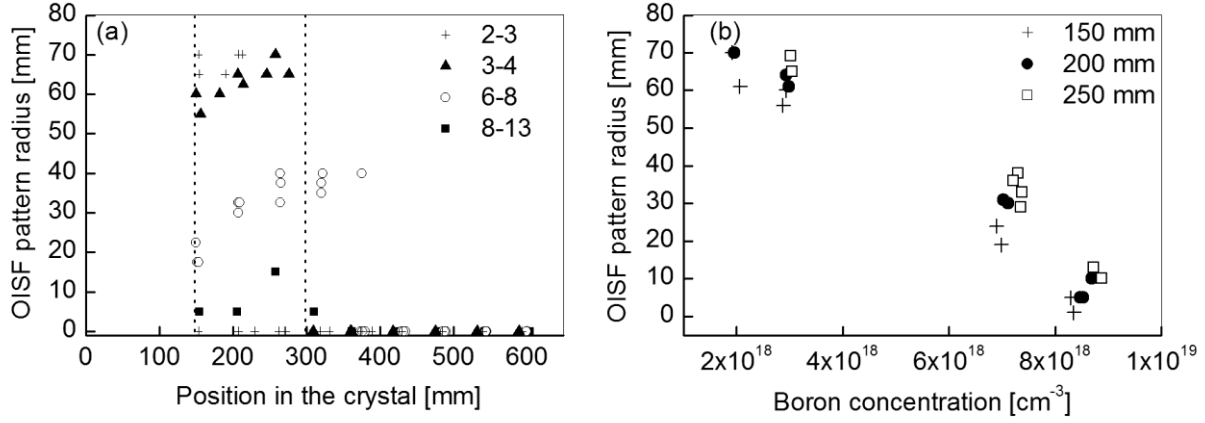


Figure 2. Measured radii of the OISF pattern after data filtering and differentiation according to the resistivity. Data for the first 150 mm were missing as this material was not used for production and, hence, was not sampled. Legend shows boron concentration in the crystals in [ $10^{18} \text{ cm}^{-3}$ ]. Each resistivity range contains data from various crystals grown by the same process with the same amount of dopant introduced into the melt. Zero values represent cases when the radius of the pattern could not be determined due to low OISF density or the wafer was OISF-free. The dotted vertical lines at 150 and 300 mm highlight the range to be compared to Fig. 3. (b) Radius of the OISF pattern as the function of boron concentration for three positions in the crystals. Legend shows the distance from the seed end.

on boron concentration and position in the crystal suggest possible relation to the vacancy-interstitial (V-I) boundary.

### 3.4 SIMULATION OF THE V-I BOUNDARY

In order to analyze the possible relation of the OISF pattern to the V-I boundary, information on the V-I boundary must be acquired. We performed computer simulations of the crystal growth process to model the temperature field in the growing crystal. Process simulations were performed for several stages of the crystal growth corresponding to the crystal length of 50, 100, 150, ... 500 mm (full crystal length is about 620 mm). The simulations yield a radial profile  $G(r)$  of the axial temperature gradient  $G$  for the various growth stages. Using the known values of the crystal pull rate  $v$  for each growth stage it was possible to construct a map of the  $v/G$  parameter over the whole crystal. The function  $v/G(L)$ , where  $L$  is distance from the crystal seed-end is shown in Fig. 3.

Let us suppose that the critical value  $v/G_{crit}$  is constant along the crystal. This assumption is valid for the lightly doped crystals where the dependence on boron concentration is weak [4, 5]. In such case the isolines of  $v/G(r, L)$  drawn in Fig. 3 correspond to the position of the V-I boundary in the crystal for labeled values of the  $v/G_{crit}$ . Comparing the region of axial position of 150–300 mm in Fig. 3 and Fig. 2a, one can recognize the similarity of the observed radius of the OISF pattern with the modeled radius of the V-I boundary. Radius of the OISF pattern for the boron doping of 2–3, 3–4 and 6–8  $\times 10^{18} \text{ cm}^{-3}$  increases from the value at 150 mm

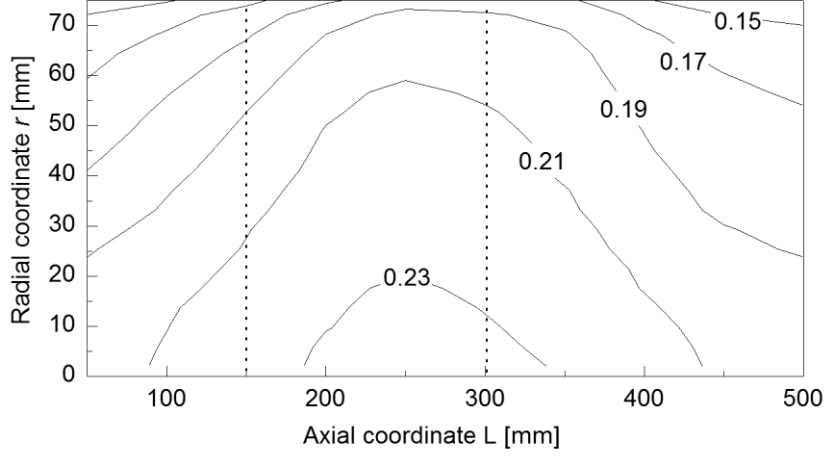


Figure 3: Map of the  $v/G$  parameter over the crystal constructed using computer simulations of crystal growth. The isolines are labeled with the corresponding value of  $v/G$  in  $[\text{mm}^2/\text{min K}]$ . The dotted vertical lines at 150 and 300 mm highlight the range to be compared to Fig. 2.

to the value at 300 mm similarly to the V-I boundary corresponding to the  $v/G_{crit}$  values of 0.17, 0.19 and 0.21  $\text{mm}^2/\text{minK}$ . We will therefore assume that the observed distribution of OISF has a relation to the V-I boundary and we will apply the theory of V-I boundary and  $v/G_{crit}$  parameter to describe the observed OISF pattern. We will temporarily suppose that the V-I boundary lies very close to the outer perimeter of the OISF pattern similarly to the OISF ring.

### 3.5 ESTIMATION OF THE CRITICAL VALUE $V/G$

Supposing that the V-I boundary lies very close to the outer perimeter of the OISF pattern (with radius  $r_{OISF}$ ), equation  $v/G(r_{OISF}) = v/G_{crit}$  holds. Comparison of the region of 150–300 mm in Fig. 2a and Fig. 3 shows that the values of  $v/G(r_{OISF})$  would indeed be quite close to the modeled isolines of  $v/G_{crit}$ . As the radius of the OISF pattern depends on the boron concentration (see Fig. 2b), the  $v/G_{crit}$  is also the function of boron concentration.

No OISF pattern was found on the lightly boron-doped wafers up to the boron concentration of  $1.7 \times 10^{18} \text{ cm}^{-3}$ . It can be concluded that the lightly doped crystals are fully vacancy-rich. The critical value for the lightly doped crystals must be therefore lower than the lowest value of the calculated  $v/G$  map shown in Fig. 3 which is about 0.13  $\text{mm}^2/\text{minK}$  (values in the uppermost left and right corners of the map). The OISF patterns were observed on wafers with boron concentration higher than  $1.7 \times 10^{18} \text{ cm}^{-3}$  and disappeared when boron concentration exceeded  $1.3 \times 10^{19} \text{ cm}^{-3}$ . It can be concluded that these most heavily doped crystals are fully interstitial-rich. The critical value for the most heavily doped crystals must be therefore higher than the highest value of the  $v/G$  map, which is 0.24  $\text{mm}^2/\text{minK}$  (value at about 250 mm at  $r = 0$  mm).



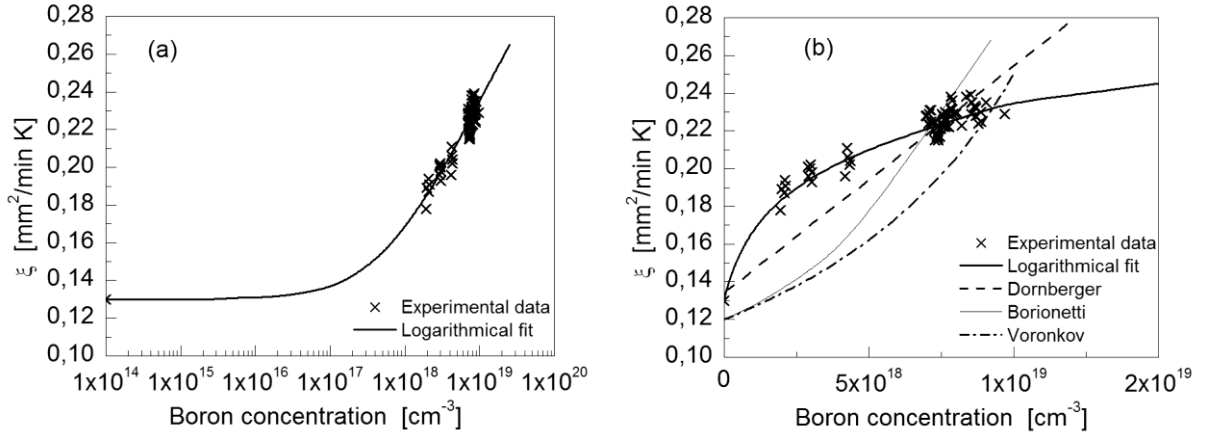


Figure 4: Critical value of  $\nu/G$  estimated from the OISF pattern radii as the function of boron concentration in (a) logarithmic and (b) linear representation concentration. The  $\nu/G_{crit} = 0.13 \text{ mm}^2/\text{min K}$  is the estimate for undoped (lightly doped) silicon. The data are approximated by the best fit according to Eq. 1. Panel (b) shows also published data by Dornberger [4], Borionetti [5] and Voronkov [6] for comparison.

Published values of the critical  $\nu/G$  value for undoped and lightly boron-doped silicon range from 0.12 to 0.14  $\text{mm}^2/\text{min K}$  [4–8]. We have chosen the value 0.13  $\text{mm}^2/\text{min K}$  which agrees to the published values as well as to the conclusion above. The values of the OISF pattern radii from Fig. 2a measured at the positions in the crystal of 150–300 mm were interpolated to obtain the radii of the OISF pattern ( $r_{OISF}$ ) for the positions of 150, 200 and 250 mm. Analogically, boron concentration  $C_B$  in the wafers corresponding to these radii was calculated. Using the condition  $\nu/G(r_{OISF}) = \nu/G_{crit}$  the critical values  $\nu/G_{crit}$  were determined from the modeled  $\nu/G(r)$  curves (these curves served for construction of the  $\nu/G$  map in Fig. 4). Assigning the values of boron concentration  $C_B$  corresponding to  $r_{OISF}$  to the critical values, the function  $\nu/G_{crit}(C_B)$  was obtained. The  $\nu/G_{crit}(C_B)$  values are plotted in Fig. 5. The best fit of the data was obtained using a logarithmical function

$$\nu / G_{crit} = a + b \ln(C_B + c) \quad (1)$$

with  $a = -1.25 \pm 0.1 \text{ mm}^2/\text{min K}$ ,  $b = -0.034 \pm 0.002 \text{ mm}^2/\text{min K}$ , and  $c = 4.8 \times 10^{17} \pm 1 \times 10^{17} \text{ cm}^{-3}$ . This empirical dependence is also shown in Fig. 4. The  $\nu/G_{crit}(C_B)$  curves reported by various authors (see Fig. 4b) differ rather significantly. We suppose that the differences are caused by the insufficient precision of the used thermal models which provide the  $G(r)$  functions.

Our results indicate that boron up to the concentration of about  $10^{17} \text{ cm}^{-3}$  does not influence the critical  $\nu/G$  value and, hence, does not influence distribution of defects in silicon crystals.

### 3.6 COMPARISON OF V-I BOUNDARY SIMULATIONS WITH OISF DISTRIBUTION

The process of growing heavily boron-doped crystals in ON Semiconductor has several variations varying by the amount of boron introduced into the melt. Each process results in a typical concentration of boron in the grown crystals. Due to segregation, boron concentration increases from the seed-end to the tail-end of the crystal. The individual growth processes therefore yield crystals of certain concentration range. The individual growth processes will be hereafter represented by the concentration range of the grown crystals (seed-end to tail-end). This representation has been already used in Fig. 2a.

Using the known resistivity axial profiles and the empirically determined function  $v/G_{crit}(C_B)$  the dependence of  $v/G_{crit}$  on the position in the crystal was determined for the growth processes displayed in Fig. 2a. Comparison with the map of  $v/G$  (Fig. 3) yields the V-I boundary radius ( $r_{V-I}$ ) as the function of position in the crystal (utilizing the condition  $v/G(r_{V-I}) = v/G_{crit}$ ). The modeled V-I boundaries are plotted in Fig. 5 together with the radii of the observed OISF patterns.

In the range of position in the crystal of about 150–300 mm, we can identify a reasonable qualitative agreement of the modeled V-I boundary radius and the measured radius of the OISF pattern. We can expect that the radius of the OISF pattern follows the V-I boundary in the beginning of the crystal where no measured data are available. The question to solve is an obvious disagreement of the V-I boundary and the OISF pattern in the second half of the crystal for boron doping below about  $6 \times 10^{18} \text{ cm}^{-3}$ . The predicted V-I boundary radius steadily decreases from its maximum at around 300 mm while the OISF pattern abruptly and completely disappears (this is represented by zero values).

The doping level of  $4\text{--}6 \times 10^{18} \text{ cm}^{-3}$  was chosen as the suitable material for further

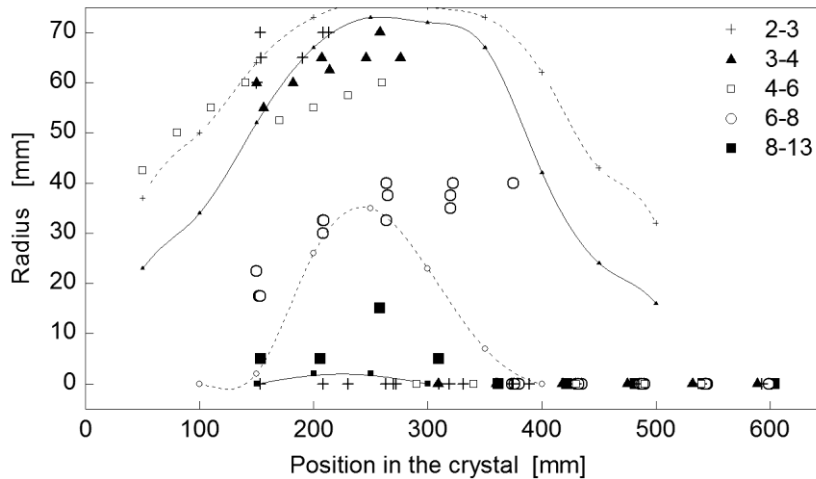


Figure 5: Measured radius of the observed OISF pattern (scattered data) and radius of the modeled V-I boundary (lines with small symbols corresponding to the doping level). The V-I boundary was modeled using the  $v/G$  map and the  $v/G_{crit}(C_B)$  function for several levels of boron doping. Legend shows boron concentration in the crystal in  $[10^{18} \text{ cm}^{-3}]$  (seed-end to tail-end).

tests. Wafers from this crystal were sampled throughout the whole crystal length and the OISF pattern was delineated. We observed that the radius of the OISF pattern steadily increases from the seed end to about 300 mm (Fig. 5) where the pattern disappeared and no OISF were found on the wafer surface. The test proved that the radius of the OISF pattern in the first half of the crystal qualitatively follows the modeled V-I boundary.

Although there are some uncertainties, the above described work shows that the OISF pattern can be qualitatively described by the  $v/G$  methodology using computer simulations of crystal growth and the empirically determined function  $v/G_{crit}(C_B)$ . The discontinuity of the radius of the OISF pattern around 150 mm observed in the case of the test crystal doped to  $4\text{--}6 \times 10^{18} \text{ cm}^{-3}$  and disappearance of the OISF pattern in the second half of all the crystals will be discussed later in section 3.13.

### 3.7 RADIAL OISF DISTRIBUTION

Key understanding of the observed OISF patterns was revealed by detailed analyses of the wafers from the test crystal doped to  $4\text{--}6 \times 10^{18} \text{ cm}^{-3}$ . OISF on the wafer surface formed circular patterns whose shape varied with the position in the crystal.

Wafers from the first quarter of the crystal (0–150 mm) show the OISF pattern consisting of the central circle and an outer ring of high OISF density which are separated by a ring of very low OISF density. Essentially no OISF were found outside the outer ring. The pattern is shown in Fig. 6a. The OISF density inside the central circle decreases from the rim to the center. Surface density of OISF was measured using the optical microscope. Fig. 6c shows the radial profile corresponding to Fig. 6a. Both Fig. 6a and Fig. 6c show that on some wafers it was possible to distinguish a fine substructure of the outer ring of OISF which was formed by two narrow rings of very high OISF density separated by a ring of slightly lower OISF density.

Wafers from the second quarter of the crystal (150–300 mm) show the OISF pattern formed only by the central circle (Fig. 6b). The OISF density inside the circle decreases from the rim to the center similarly to the inner circle found on the wafers from the first quarter of the crystal. OISF density outside the circle is essentially zero.

The OISF density observed on the wafers from the test crystal doped to  $4\text{--}6 \times 10^{18} \text{ cm}^{-3}$  generally decreases with the distance from the crystal seed-end. The OISF pattern so becomes less and less sharp, the radius becomes less and less measurable and finally no OISF are found on the wafers in the second half of the crystal.

Fig. 6e shows the radii of the measurable OISF patterns. The plot shows radius  $r_1$  of the outer ring and radius  $r_2$  of the inner circle found on the wafers from the first crystal quarter and radius  $r_3$  of the circle observed on the wafers from the second quarter of the crystal. The radii are plotted as the function of distance from the seed-end (denoted as  $L$ ). It is apparent that the  $r_3(L)$  curve is the follow-up of the  $r_2(L)$

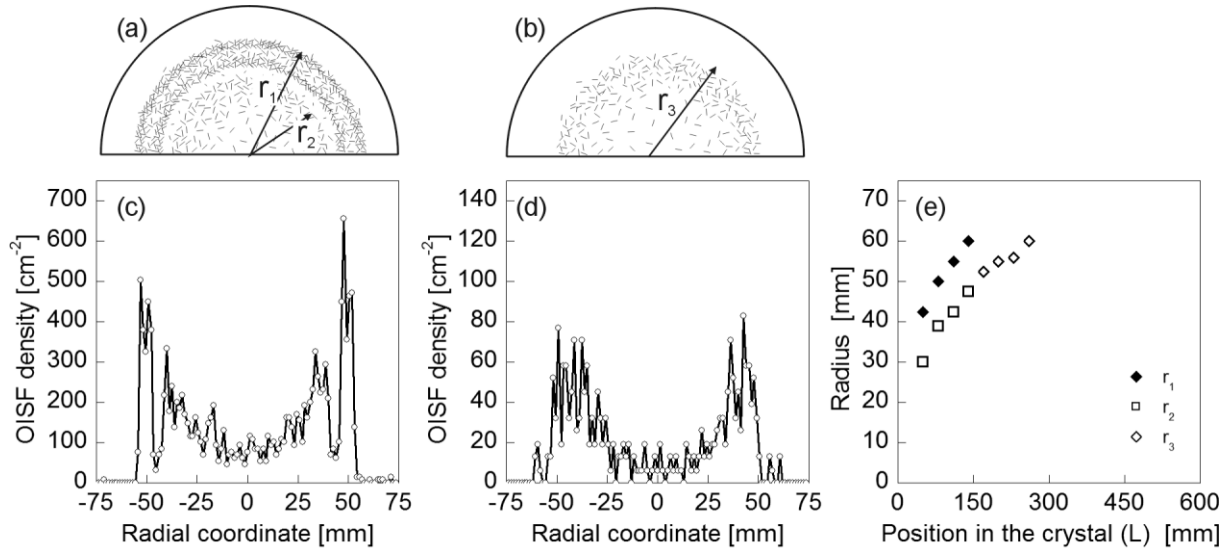


Figure 6: Scheme of the OISF pattern observed on the wafers from (a) the first and (b) the second quarter of the crystal (only half of the wafer is shown). Panels (c) and (d) show radial profiles of the surface density of OISF observed on the wafers represented by panels (a) and (b), respectively. Note different scales on the y-axis demonstrating the decrease in OISF density along the crystal. Panel (e) shows the radius of the features forming the OISF pattern. Labeling  $r_1$ ,  $r_2$ ,  $r_3$  corresponds to panels (a) and (b).

curve. As the circles of OISF corresponding to  $r_2(L)$  and  $r_3(L)$  show also similar radial dependence of OISF density, it opens that it is a case of the same feature.

Considering the above discussed results we can formulate a hypothesis that the OISF pattern observed in the first quarter of the crystal is the complete pattern, which would appear throughout the whole crystal under optimal circumstances. However, due to decreasing OISF density, the pattern gradually disappears with increasing distance from the crystal seed-end. The outer ring disappears first, the inner circle follows. This scenario is supported by the trace of the outer ring captured at the radius of about 60 mm in Fig. 6d, which was not distinguishable by eye on the wafer (as sketched in Fig. 6b). The reason for decrease in the OISF density with the distance from the seed end is to be resolved (see section 3.13).

### 3.8 RELATION OF OISF TO BULK CRYSTAL DEFECTS

It is known that the OISF ring is formed by nucleation of the stacking faults on oxide precipitates. It is therefore likely that the observed OISF pattern also delineates oxide precipitates in the wafer. Distribution of the oxide precipitates in the bulk of the wafers was studied by the X-ray section topography.

Fig. 7a shows the X-ray section topogram of the region of the outer ring of OISF found on the wafer from the first crystal quarter. Oxide precipitates are visible as black dots. The topogram clearly shows non-homogeneous distribution of oxide precipitates depending on the radial position on the wafer. Radial profile of the precipitate density is plotted in Fig. 7b together with the radial profile

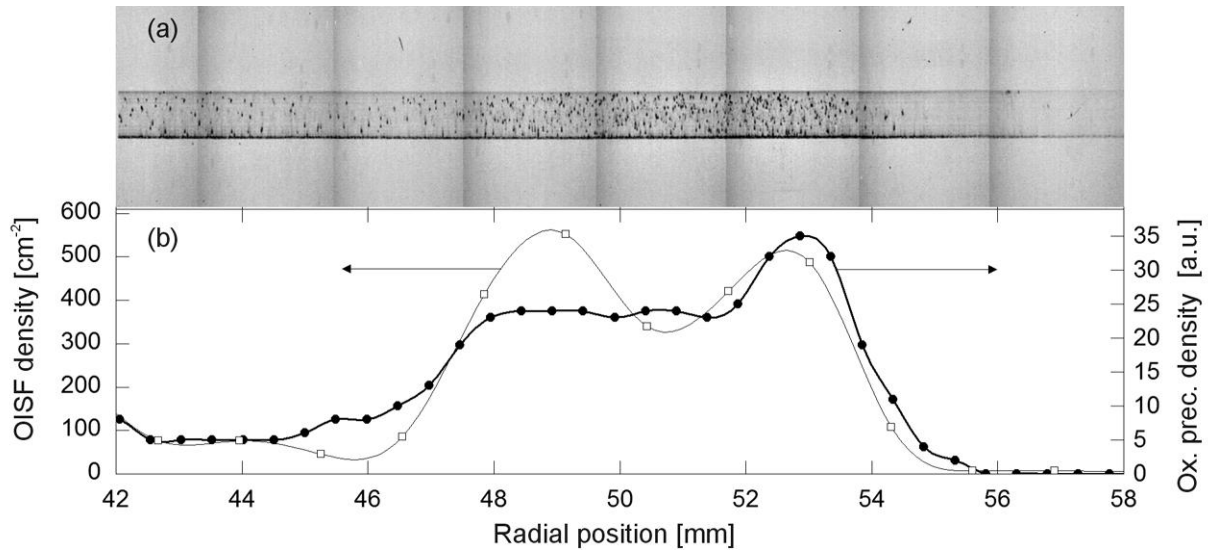


Figure 7: (a) X-ray section topogram of the wafer from the first crystal quarter after the OISF test. The topogram shows the region of the outer ring. Picture dimensions are not to scale. (b) Surface density of OISF from Fig. 6c (open symbols) and bulk density of oxide precipitates counted from the topogram (full symbols). The radial coordinate represents the distance from the wafer center.

of the OISF density from Fig. 6c. Correlation of the two radial profiles is obvious — both curves show the highest values in the region of about 47–54 mm from the wafer center, lower values closer to wafer center and zero values closer to wafer rim.

It can be therefore concluded that the OISF forming the pattern on the surface of our heavily boron-doped wafers nucleate on oxide precipitates located in the near-surface region of the wafer. As the OISF test is the only thermal operation applied to the test wafers, the oxide precipitates certainly nucleated during the crystal growth (nucleation during the OISF test is negligible). These precipitates will be called the grown-in precipitates. Their ability to serve as the nuclei for OISF implies that their size after the crystal growth is larger than the critical radius at the temperature of the OISF test. In other words the OISF pattern is formed by nucleation of OISF on the grown-in oxide precipitates which are supercritical at the temperature of the OISF test.

### 3.9 ORIGIN OF THE RADIAL OISF PATTERN

It is known that precipitation of oxygen is supported by the presence of vacancies in the material. According to the Voronkov theory [8, 9], interactions of point defects during the crystal growth result in the radial profile of concentration of free vacancies showing a double-peak close to the V-I boundary. This distribution of vacancies results in a typical radial distribution of oxide precipitates (Fig. 8c). Comparing these profiles with Fig. 6c, one can recognize apparent similarity of the OISF profiles with the profile of residual vacancies and small oxide precipitates.

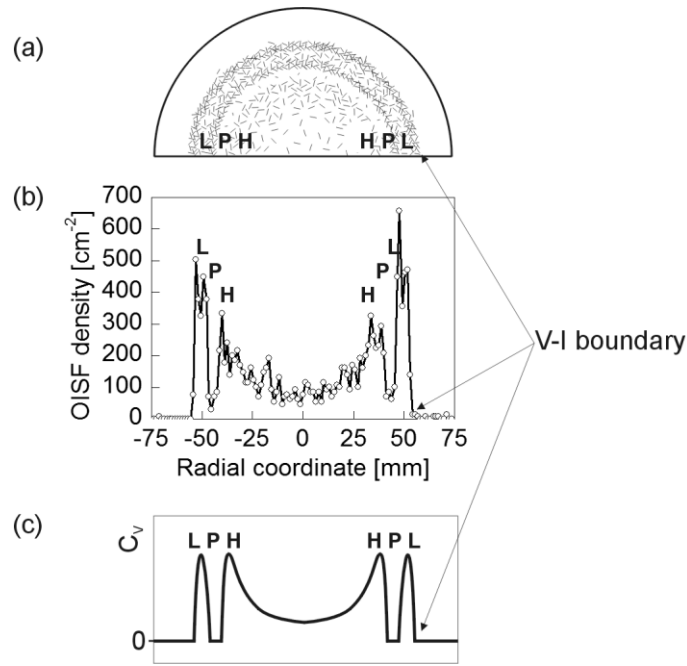


Figure 8: The figure demonstrates the relation of the OISF pattern to the microdefect bands and V-I boundary. (a) Typical distribution of OISF on the surface of wafers from the first quarter of the heavily boron-doped crystals. (b) Radial profile of the OISF surface density corresponding to the wafer from panel (a). (c) Schematic representation of the radial profile of concentration of free vacancies (or small oxide precipitates) established typically in lightly boron-doped silicon crystal. Microdefect bands and the V-I boundary are labeled in the picture

We will compare Fig. 6a,c with Fig. 8c which describes the typical distribution of crystal defects in lightly boron-doped silicon crystals. The similarity of the profiles allows us to identify the key features of the OISF pattern. The deduced relations are shown in Fig. 8. We believe that:

1. the outer rim of the OISF pattern coincides with the V-I boundary; the interior is the vacancy-rich core and the exterior is the interstitial-rich region;
2. the outer ring of very high OISF density coincides with the L-band;
3. the region of the highest OISF density in the central circle (close to its outer rim) coincides with the H-band;
4. the ring of low OISF density separating the L- and H- bands corresponds to the P-band.

Let us remind that we showed in the previous section that the OISF observed on the surface of our wafers reflect the distribution of grown-in oxide precipitates supercritical at the temperature of the OISF test, which was  $1150^\circ\text{C}$  in this case. The above stated conclusions mean that the oxide precipitates formed in the L- and H- bands during the crystal growth are larger than the critical radius at  $1150^\circ\text{C}$  which is a very unusual phenomenon. The L- and H- bands typically contain small grown-in precipitates, and OISF are formed only in the P-band. We see seemingly inverse behavior when OISF are formed in the L- and H- bands in higher density

than in the P-band. However, as the OISF density in the P-band is nonzero (see Fig. 6c), the observed phenomenon is rather an addition of strong oxygen precipitation in the L- and H- bands superimposed over the usual OISF formation in the P-band.

### 3.10 VERIFICATION OF THE V-I BOUNDARY

The vacancy-rich core of the crystal is characterized by the presence of the vacancy-type defects — voids and COPs. The outer boundary of the COP-containing region is found close to the V-I boundary, usually it is located in the P-band [10, 11] as shown in Fig. 18b. The COP test can be therefore used for delineation of the V-I boundary, more specifically of the OISF ring.

The COP test was performed on our wafers throughout the whole crystal. The COPs were clearly delineated in compact circles in the center of the wafers; rim of the wafers was COP-free. Radius of the COP region was measured from the COP maps.

Fig. 9 shows the radius of the COP-containing region found on the analyzed wafers together with the radii of the OSF pattern reprinted from Fig. 6e. Let us first explore the region of 0–150 mm. The radius of the COP region lies between the radii of the L- and H- bands determined from the OISF pattern. Hence, the radius of the COP region coincides with the estimated position of the P-band. This fact validates the correct identification of the bands and the V-I boundary.

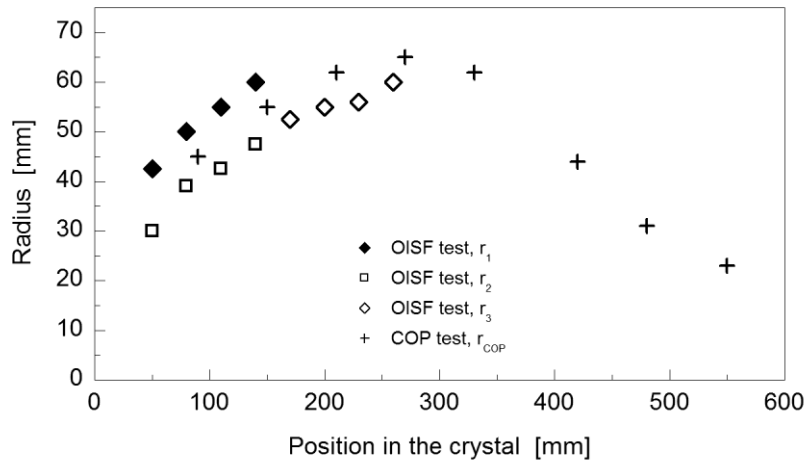


Figure 9: The radii of the features of the OISF pattern (labeled according to Fig. 6) and radius of the COP ( $r_{COP}$ ) region as the function of position in the crystal.

### 3.11 ORIGIN OF THE AXIAL CHANGES IN THE OISF PATTERN

The identification of the bands in the first crystal quarter as shown in Fig. 8 seems to be very consistent. As the P-band delineated by the COP test was found throughout the whole crystal (see Fig. 9), we expect that also the V-I boundary and all the microdefect bands go through the whole crystal. This assumption is supported

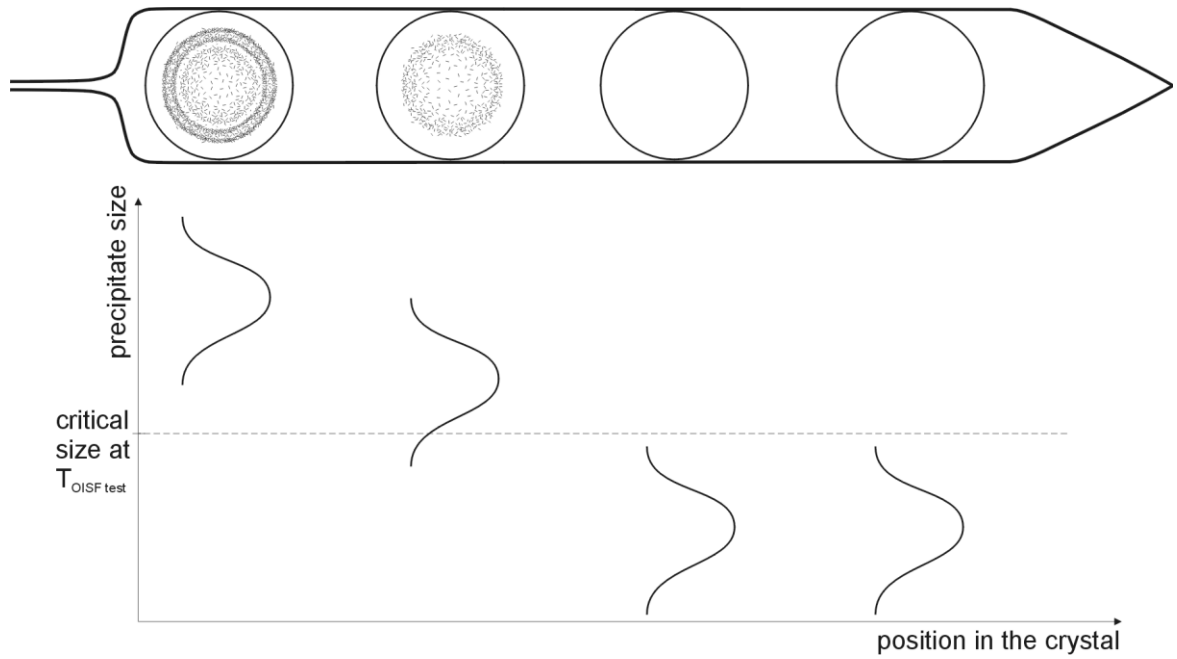


Figure 10: Top: Illustration of the OISF pattern observed in various positions in the crystal. Bottom: Proposed distribution curves of the size of the grown-in oxide precipitates corresponding to various positions in the crystal and their relation to the critical radius at the temperature of the OISF test.

by observation of the H-band of the radius  $r_3$  found in the second quarter of the crystal (150–300 mm).

However, if the L-, P- and H-bands go through the whole crystal, there is a question why they are not delineated by the OISF pattern. To deduce the reason we will now analyze the mechanism of OISF formation.

It was shown (section 3.8) that OISF observed on the surface of the wafer nucleate on oxide precipitates located near the surface. In general, oxide precipitates smaller than the critical radius at the temperature of the OISF test quickly dissolve during the temperature ramp-up or early after the temperature is achieved and can not serve as the nuclei for OISF growth.

Let us suppose that the size of the grown-in oxide precipitates is not homogeneous throughout the crystal and that it decreases from the crystal seed-end to the tail-end. We can imagine that the distribution curve of precipitate size shifts to lower values with increasing distance from the seed-end. This situation is schematically demonstrated in Fig. 10. With increasing distance from the seed-end larger portion of the distribution curves falls below the critical radius corresponding to the temperature of the OISF test. Simultaneously, larger portion of the precipitates becomes undercritical and dissolves. The OISF density therefore decreases and finally no OISF are formed on the surface because all oxide precipitates are dissolved.

Indeed, this proposed scenario corresponds to the observed behavior of the OISF pattern. As the L-band vanishes earlier than the H-band, it is likely that the grown-in oxide precipitates in the H-band are larger compared to those in the L-band.



### 3.12 OISF TEST WITH PRE-ANNEALING

We designed a test to verify the mechanism of axial disappearance of the OISF pattern proposed in section 3.11. A set of wafers was annealed prior the OISF test at 1050°C for 16 h. The annealing temperature was chosen to be above the typical range for nucleation of new oxide precipitates (which is about 500–900°C) and below the typical temperature of the OISF test (which is usually 1100–1150 °C). The grown-in oxide precipitates were therefore allowed to grow while no new precipitates should be nucleated.

Indeed, we observed formation of OISF on the wafers from the whole crystal. Radius of the OISF region observed during this test is plotted in Fig. 11. It is shown that this radius coincides with the outer radius of the L-band in the first crystal quarter (OISF test  $r_1$ , i.e., the V-I boundary) and follows the radius of the P-band delineated by the COP test throughout the whole crystal. It is obvious that the test revealed the V-I boundary in the whole crystal and verified the assumption on the varying size of grown-in oxide precipitates along the crystal. The results are finally consistent with the results of computer simulations which predict the V-I boundary in the whole crystal (see section 3.4).

However, we have to note few peculiarities of the results. The banded structure was lost and only a full ring of OISF was observed throughout the crystal. As the outer diameter of the OISF region in the first crystal quarter coincides with the outer diameter of the L-band and therefore with the V-I boundary, it is obvious that OISF were formed in the whole vacancy-rich region. As the outer diameter of the full OISF region is larger than the COP region (and rather equidistantly spaced) throughout the whole crystal, we can conclude that OISF were formed in the vacancy-rich region in the whole crystal. Considering the applied pre-annealing this can be explained in a way that the grown-in oxide precipitates were

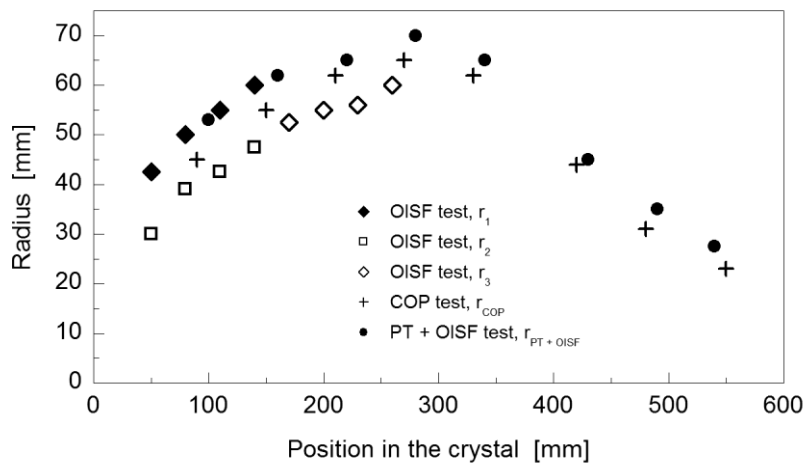


Figure 11: The radii of the features of the OISF pattern (labeled according to Fig. 6), radius of the COP region and outer radius of the OISF pattern observed after OISF test with pre-annealing ( $r_{PT+OISF}$ ) as the function of position in the crystal.

supercritical at 1050°C in the whole vacancy-rich region throughout the whole crystal.

Another peculiarity was that the OISF ring in the first crystal quarter was difficult to resolve after pre-annealing. The reason was a large amount of smaller OISF (5–15  $\mu\text{m}$ ) and etch pits over the whole wafer surface. The OISF pattern itself was formed by large OISF (20–30  $\mu\text{m}$ ). Formation of etch pits and OISF over the whole wafer surface suggests that huge oxygen precipitation occurred even in the interstitial-rich region outside the OISF pattern where it is usually suppressed.

Oxygen precipitation in both vacancy- and interstitial-type crystal was observed by Kim et al. [13]. Heavily boron-doped wafers of both interstitial-type and mixed-type were examined by heat treatment and OISF test. While BMD (Bulk Micro Defects), i.e., oxygen precipitates, of high density were observed both in the vacancy- and interstitial-type regions, OISF were observed in most cases only in the OISF ring region as in the case of the lightly doped silicon. However, after pre-annealing at 900°C, OISF were formed over the entire wafer surface regardless of the wafer type. Unlike in our case, precipitates observed by Kim et al. were not stable enough at higher temperature. Above 1000°C OISF were observed only in the OISF ring again.

Asayama et al. [14] also observed BMD formation over the entire wafer surface regardless of the defect region type. Similarly to Kim et al., the precipitates in the OISF ring showed the highest stability at high temperature. Both these results (a) partly agree and (b) partly disagree with our observations.

ad a) Agreement with our results: Kim and Asayama showed that high boron doping allows oxygen precipitation even in the interstitial-rich crystal region. Precipitates there, however, exhibit lower density and worse thermal stability (thus smaller size) compared to the vacancy-rich region. Grown-in precipitates in our crystals are certainly also smaller in the interstitial-rich region because after OISF test the OISF were observed only in the vacancy-rich region. Behavior of our wafers after pre-annealing is also in accordance with findings of Kim and Asayama. In the first crystal quarter we observed etch pits and OISF also in the interstitial-rich region. We suppose that the etch pits are delineated oxygen precipitates and that all OISF nucleate on oxygen precipitates. OISF in this region were smaller compared to the vacancy-rich region. This suggests that their growth started later because the grown-in precipitates were smaller than in the vacancy-rich region and it took more time to grow to the size large enough to serve as the OISF nuclei.

Oxygen precipitation in the interstitial-rich region can be explained as follows. The growth of an oxygen precipitate is accompanied by the emission of silicon self-interstitials. While supersaturation of oxygen is the driving force for precipitation, supersaturation of self-interstitials acts against precipitation [15]. It has been published that high boron concentration increases the equilibrium concentration of silicon self-interstitials [16], it decreases their supersaturation which in turn allows oxygen to precipitate. The first crystal quarter is characteristic by the highest oxygen concentration. We suppose that lower oxygen content in the rest

of the crystal causes lower supersaturation which cannot compete with high supersaturation of self-interstitials. Therefore, precipitation in the interstitial-rich region in the rest of the crystal is not allowed and OISF are not observed even after pre-annealing.

ad b) Disagreement with our results: In most cases reported by Kim the OISF were observed solely in the OISF ring and only pre-annealing at 900°C led to OISF formation over the entire wafer surface. In the first half of the crystal we observed OISF formation generally in the whole vacancy-rich crystal region excluding the OISF ring (P-band). The OISF over the entire surface were observed after pre-annealing at 1050°C in the first crystal quarter. Kim's wafers were doped at the same level as our wafers and they were also of the mixed type. A different behavior of the grown-in defects should be thus caused by some other parameters. We conclude these are the crystal thermal history and the oxygen content. Since no information on the thermal history was published by Kim, this parameter cannot be discussed. The oxygen concentration in the first quarter of our crystals was in the range of 30–35 ppma, while Kim reported the content of 25.5–27.5 ppma. A higher oxygen concentration is likely the root cause of the larger size of the grown-in precipitates, which enhances their stability at higher temperature.

Despite some peculiarities of the results the OISF test after pre-annealing verified our conclusions on the size distribution of the grown-in oxygen precipitate which results in changing appearance of the OISF pattern along the crystal.

### **3.13 ORIGIN OF THE AXIAL VARIATIONS IN THE SIZE OF GROWN-IN OXIDE PRECIPITATES**

In the former text we came to the conclusion that the size of the grown-in oxide precipitates in the studied crystals decreases from the seed-end to the tail-end. This size distribution results in gradual disappearance of the OISF pattern. In order to support this hypothesis we have to explain the variation of precipitate size throughout the crystal.

It is well known that the key factors controlling oxygen precipitation in the grown crystal are concentration of oxygen and time evolution of temperature, so called thermal history [15,17–21]. The window for effective precipitation of oxygen is bound by the temperature when appreciable supersaturation is achieved from the top, and by the temperature when oxygen diffusion is negligible from the bottom. Fig. 12b shows oxygen concentration typical for the studied crystals, Fig. 51a reminds the OISF pattern and Fig. 12c shows the modeled thermal history.

Considering the first three quarters of the crystal it is seen that oxygen concentration decreases while the thermal history is comparable down to about 650°C. This temperature is almost the lower limit for appreciable nucleation of oxide precipitates [18]. The lower boundary of the nucleation window is similar for the whole considered portion of the crystal as the dependence of the nucleation rate on oxygen concentration at the temperature around 650°C is weak [18]. The upper boundary of the nucleation window is determined by oxygen

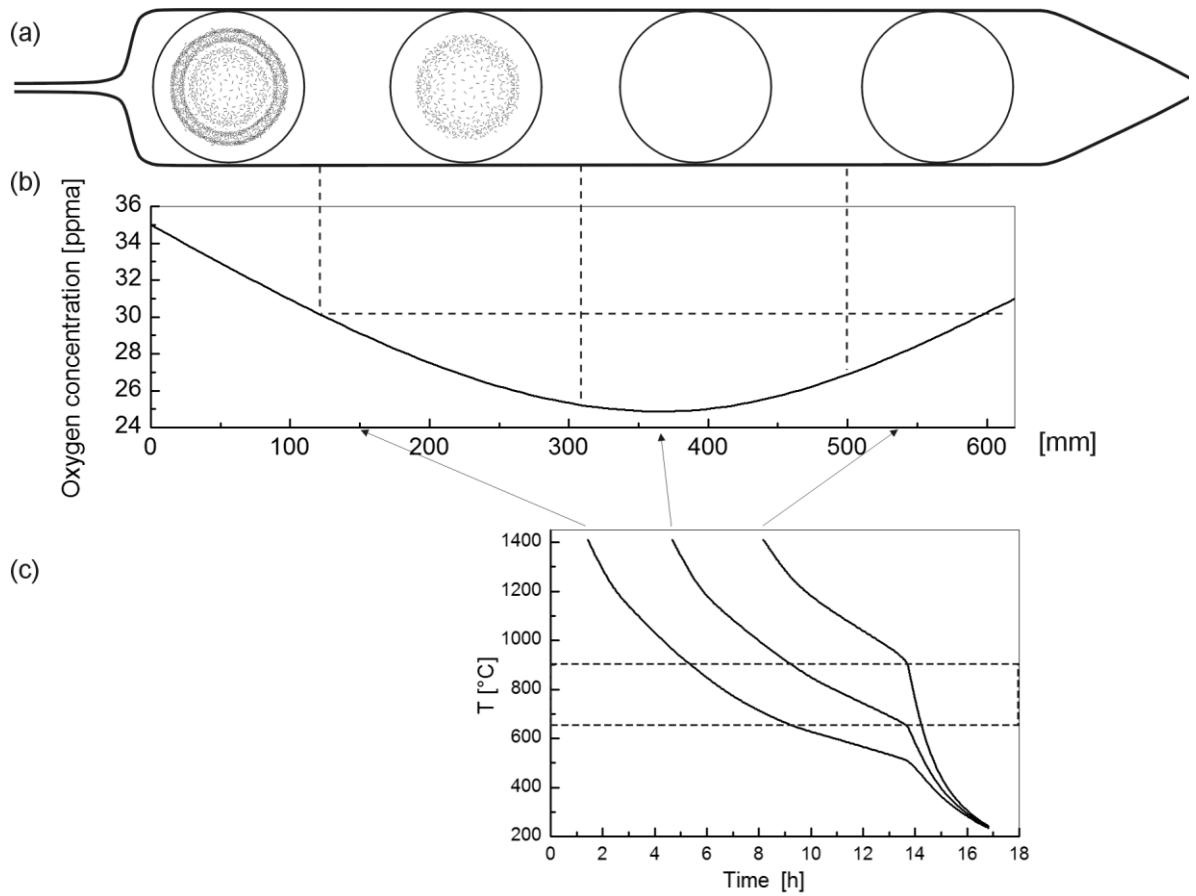


Figure 51: (a) Schematic representation of the observed OISF pattern throughout the crystal. (b) Axial profile of oxygen concentration in the crystal. (c) Thermal history modeled for three positions in the crystal shown by arrows.

concentration. As the oxygen content decreases the temperature of supersaturation shifts to lower values and consequently the time for the growth of oxide precipitates is shortened compared to higher oxygen levels. Decreasing oxygen concentration therefore results in reduction of size of the grown-in oxide precipitates. This scenario corresponds to the observed disappearance of the OISF pattern.

Oxygen concentration in the fourth quarter of the crystal rises again to the level of the second crystal quarter. However, while the OISF pattern is observed in the second quarter, no OISF pattern has been found in the fourth quarter. This phenomenon can be explained on the basis of the thermal history. Temperature evolution in these two crystal portions of essentially the same oxygen content differs as it is shown in Fig. 51c. It has been reported in [187] that the critical temperature range for formation of oxide precipitates during the crystal growth is about 900–600°C. Fig. 12c shows that it is almost precisely this range where thermal history of the fourth crystal quarter differs from the rest of the crystal. After the growth of the crystal is completed, the crystal is detached from the melt and rather quickly cooled. While most of the crystal body dwells already at rather low temperature (around or below 650°C), the tail-end of the crystal (the fourth quarter) experiences

fast cooling from about 900°C. It is clear from Fig. 12c that the dwell time in the temperature range of 900–650°C is substantially shorter in the fourth crystal quarter compared to the rest of the crystal (approximately four times). As the result, one can expect formation of substantially smaller grown-in oxide precipitates in the fourth crystal quarter compared to the second quarter, despite the oxygen concentration in these crystal portions is the same.

Thus, the variation of size of the grown-in oxide precipitates along the crystal leading to the observed variation of the OISF pattern can be explained in terms of the axial profile of oxygen concentration and the crystal thermal history.

### 3.14 SUMMARY ON FORMATION OF THE OISF PATTERN

Taking the above discussed mechanisms into account we can compile a consistent model qualitatively describing formation of crystal defects in our heavily boron-doped crystals:

1. The critical value of  $v/G$  is the function of boron concentration in the crystal; it can be expressed as the empirical logarithmical function (Eq. 1).
2. Lightly doped crystals are fully vacancy-rich; heavily doped crystals (boron concentration in the range of  $1.7 \times 10^{18}$ – $1.3 \times 10^{19} \text{ cm}^{-3}$ ) are of the mixed type and contain the V-I boundary; the most heavily doped crystals are fully interstitial-rich.
3. Formation of crystal defects from the crystallization temperature down to about 900°C is described by the Voronkov theory. These processes result in a double peak radial profile of residual vacancies.
4. Residual vacancies assist in formation of the grown-in oxide precipitates during further cooling of the crystal. The density of the precipitates is proportional to concentration of vacancies. The highest density is achieved in the L- and H- bands; the density in the P-band and in the central region bound by the H-band is lower and no oxide precipitates are formed outside the V-I boundary, i.e. in the interstitial-rich region.
5. Oxide precipitates formed in the first crystal quarter reach the size which is supercritical at the temperature of the OISF test (1150°C) and serve as the nucleation sites for OISF. The surface density of OISF reflects the bulk density of the grown-in precipitates. The resulting OISF pattern therefore reveals the V-I boundary and the L-, P- and H- bands in the vacancy-rich core.
6. The size of the grown-in oxide precipitates decreases with the distance from the seed-end as the consequence of decreasing oxygen concentration. As the size distribution curve shifts below the value of the critical radius of the nuclei at the temperature of the OISF test, larger amount of the grown-in precipitates dissolves and the OISF density decreases. The OISF pattern therefore gradually vanishes with increasing distance from the seed-end. As the L-band disappears sooner, the size of the precipitates in the L-band seems to be smaller compared to the H-band.

7. The size of the grown-in oxide precipitates in the tail-end of the crystal is reduced as the consequence of the faster cooling in the temperature range of about 900–650°C. Therefore no OISF are formed in this crystal portion despite the oxygen concentration level sufficient for formation of stable OISF nuclei.

### 3.15 ENHANCED PRECIPITATION OF OXYGEN

The OISF ring is formed on the wafers as the consequence of the fact that only the grown-in oxide precipitates in the P-band are supercritical at the temperature of the OISF test. In our case we see formation of supercritical precipitates especially in the L- and H- bands. Hence, oxygen precipitation in these bands is unusually strong. We reported on this phenomenon in [22, 23] and call it enhanced oxygen precipitation.

The observed OISF pattern following the radial profile of residual vacancies has not been published previously. The published data [12, 13, 24-27] report on formation of the OISF ring in the P-band. Parameters of the crystals studied in this work were compared to the data of other authors who also studied oxygen precipitation and OISF formation in heavily boron-doped silicon. While Dornberger [24] does not specify oxygen concentration in studied crystals, Kim et al. [13] report oxygen concentration of 26–28 ppma. Suhren [12] reports the oxygen content in the range of 23.5–35.5 ppma for 200 mm and 125 mm processes, but it is not clear what combinations of boron and oxygen concentration were studied. Oxygen concentration in the first crystal quarter of our crystals (where the complete OISF pattern and strongest oxygen precipitation is observed) is 29–35 ppma. This high value is likely the reason for the enhanced oxygen precipitation. However, the high oxygen concentration itself can not be the root cause as the standard OISF ring is observed in lightly doped crystals with the same oxygen content [25]. We can conclude that the enhanced oxygen precipitation observed in the L- and H- bands is the consequence of the combination of the high oxygen concentration, high boron concentration and suitable thermal history.

It was shown in section 3.9 that spatial distribution of the supercritical grown-in precipitates follows the radial profile of the residual vacancies. This profile is established around 900°C. The temperature of about 600°C can be considered as the lower limit below which formation of grown-in oxide precipitates is negligible due to very low oxygen diffusivity. Hence, enhanced precipitation of oxygen during the growth of the heavily boron-doped silicon crystals occurs in the temperature range of about 900–650°C.

The schematic summary of our understanding of defect formation in boron doped silicon is presented in the following scenario:

- Lightly boron-doped crystals with a low oxygen concentration — formation of grown-in oxide precipitates is generally suppressed.
- Lightly boron-doped crystals with a sufficient oxygen concentration — small grown-in oxide precipitates are formed in the L- and H-band, large grown-in

oxide precipitates are formed in the P-band. The precipitate density in the P-band is lower than in the L- and H-band.

- Heavily boron-doped crystals with a low oxygen concentration — formation of grown-in oxide precipitates is generally suppressed.
- Heavily boron-doped crystals with an intermediate oxygen concentration — large grown-in oxide precipitates are formed in the H-band and its interior.
- Heavily boron-doped crystals with a high oxygen concentration — large grown-in oxide precipitates are formed essentially in the whole vacancy-rich region. The precipitate density in the P-band and interior of the H-band is lower than in the L- and H-band.

### 3.16 INFLUENCE OF BORON ON OXYGEN PRECIPITATION

Several mechanisms of the influence of boron doping on formation of crystal defects have been discussed in published papers.

In our previous work [22, 23] and section 3.12 we adopted the mechanism when the strain of the growing oxide precipitate is relieved by emission of silicon interstitials and we referred to a work of Ishikawa [16] showing increased equilibrium of self interstitials at higher boron concentration to explain oxygen precipitation in the interstitial-rich region. Other mechanisms of boron influence on defect formation have also been published.

Storage and release of silicon interstitials in boron-interstitial pairs was modeled by Sinno et al. [28]. It was shown that the position of the OISF ring is a function of boron concentration and can be explained by storage of silicon interstitials in BI and B<sub>2</sub>I pairs at high temperatures. As free interstitials are consumed during recombination with vacancies, the boron-interstitial pairs start to dissociate and new interstitials are released into the lattice. These extra interstitials recombine with remaining vacancies. The V-I boundary thus shift to the originally vacancy-rich region. In other words, the OISF ring shrinks with increasing boron concentration.

Electronic shift effect on equilibrium concentrations of intrinsic point defects was proposed by Voronkov and Falster [6]. Substitutional boron in the silicon lattice induces a shift in the electron concentration with respect to the intrinsic value. The shifted electron concentration is proportional to boron concentration. As vacancies in silicon are assumed to be single negatively charged, their concentration is influenced by the concentration of free electrons. Taking the law of mass action into consideration it follows that the equilibrium concentration of charged vacancies is shifted in inverse proportion to the concentration of boron. The increasing boron concentration (leading to decreased vacancy concentration) therefore results in shifting of the V-I boundary to the originally vacancy-rich region and shrinking of the OISF ring.

FTIR analyses of oxide precipitates performed by De Gryse et al. [29] indicate that the chemical composition of the precipitates varies with boron concentration. While oxide precipitates in the lightly boron-doped silicon consist of a mixture of SiO<sub>2</sub> and Si, a mixture of SiO<sub>2</sub> and B<sub>2</sub>O<sub>3</sub> was identified in the precipitates

in the heavily boron-doped silicon. The fraction of  $B_2O_3$  was up to 40% of the precipitate volume in the material doped to about  $8\text{ m}\Omega\text{ cm}$ . Due to lower bulk modulus of  $B_2O_3$  oxide precipitates in heavily doped silicon are more easily compressed which has implications for the injection of silicon interstitials into the lattice. It can be concluded that the growth of oxide precipitates in heavily boron-doped silicon is enhanced due to lower emission of silicon interstitials into surrounding lattice.

Reduction of the strain related to the precipitate growth in heavily boron-doped silicon was indicated also by Ono et al. [30] as the result of boron segregation into oxide precipitates. Smaller boron atoms incorporated into the precipitate instead of silicon provide free space for the precipitate growth. Oxygen precipitation in heavily boron-doped silicon is therefore easier compared to the lightly doped material. The effect of stress relief by boron incorporation was simulated with good agreement to the experimental data [31].

Other mechanisms influencing formation of crystal defects in heavily-boron doped silicon were also proposed such as clustering of boron atoms and oxygen which reduces the concentration of interstitial oxygen [32, 33] and thermal donor formation [34, 35]. These do not seem to be much probable and are not further considered in this work.

The mechanisms of boron-interstitial pairing and electronic shift effect were discussed only with respect to establishment of the V-I boundary during the recombination stage of defect formation [6, 28, 36]. On the other hand the effect of strain relief by boron incorporation into the precipitates was studied while the nature of the material (vacancy-rich or interstitial-rich material) and the influence on the V-I boundary were not considered. The older works have to be considered carefully in general because the authors did not consider vacancy-rich and interstitial-rich material (which is a critical factor) at that time.

Although the mechanism of boron influence on formation of defects in silicon remains uncertain, the basic feature is generally accepted — formation of an oxide precipitate is accompanied by formation of strain which has to be relieved in order to allow the precipitate to grow. As concluded in section 3.13 enhancement of precipitation in the L- and H-band occurs at lower temperatures (roughly  $900\text{--}650^\circ\text{C}$ ). At these temperatures the suppressed emission of silicon interstitials due to low equilibrium concentration of interstitials is the main force acting against precipitate growth. Let us discuss the possible mechanisms of enhanced emission of interstitials:

- As the equilibrium concentration of boron-interstitial pairs is an increasing function of temperature [28], the population of the BI and  $B_2I$  pairs at lower temperature would be saturated by the pairs formed at higher temperature. Formation of new pairs would therefore be suppressed. Besides, decomposition of the boron-interstitial pairs would tend to add interstitials into the lattice. This effect would act against emission of next interstitials



from the precipitate. Therefore, boron-interstitial pairing seems not to be the reason for enhanced oxygen precipitation.

- The decreased vacancy concentration due to the electronic shift effect would modify radial position of microdefect bands. To be more precise the microdefect bands would move towards the V-I boundary and the diameter of the void-containing region would increase because the same vacancy supersaturation would be achieved for lower vacancy concentration. The reason arises from the fact that vacancy supersaturation is the driving force for void formation and is also considered as the supportive driving force for oxygen precipitation in Voronkov's models [10, 11]. The defect formation at higher temperatures would be enhanced due to increased vacancy supersaturation and the concentration of residual vacancies would decrease consequently. This effect would act against formation of the grown-in oxygen precipitates below 900°C.
- The increased equilibrium concentration of silicon interstitials would enhance emission of interstitials by decreased interstitial supersaturation. This effect can enhance oxygen precipitation.
- Incorporation of boron into the precipitate would decrease number of emitted interstitials per size increment. The increase of interstitial supersaturation would be slowed down and precipitation would be enhanced.

Although the position of the V-I boundary was explained by the electronic shift [6] and boron-interstitial pairing [28], it seems that these effects cannot be the root cause of enhanced precipitation of oxygen at lower temperatures. On the other hand the influence of boron on the equilibrium concentration of interstitials [16] or boron incorporation into the oxide precipitates [29–31] might be responsible for enhanced precipitation of oxygen in heavily boron-doped silicon.

## 4 SUMMARY

This work is focused on the study of the crystal defects in silicon single crystals, particularly in silicon crystals doped with boron.

An unusual distribution of oxidation induced stacking faults (OISFs) was observed on the surface of heavily boron-doped wafers. The author performed a detailed analysis of the OISF distribution over a wide range of boron doping levels. The analysis revealed circular OISF patterns whose shape varied as the function of doping level and position in the crystal. The full pattern consisting of a thin ring of OISFs outside a full circle of OISFs is formed in the crystal beginning. The observed OISF patterns have not been published before.

The author identified a qualitative agreement between the radial profile of OISF surface density and the radial profile of residual vacancies described by the model published by other authors. This correlation enabled identification of specific bands of crystal defect within the OISF pattern. The so called H-, P-, and L-bands were identified as well as the vacancy-interstitial (V-I) boundary.

The correct identification of the V-I boundary was experimentally verified by delineation of vacancy type bulk defects — the COPs. Computer simulations of crystal growth were utilized for modeling of the V-I boundary in the crystal. The critical  $v/G$  parameter was determined as the function of boron concentration using the measured radii of the OISF patterns. A reasonable quantitative agreement of the modeled V-I boundary and defect distribution in the crystals was achieved.

Based on the results of X-ray section topography and a specific OISF test with pre-annealing the author showed that the oxide precipitates formed during the crystal growth — the grown-in precipitates — are the nuclei for the OISFs observed on the wafer surface. The observed changes in the OISF pattern were explained on the basis of oxygen precipitation dependent on the position in the crystal. This dependence was explicated in terms of oxygen concentration and thermal history.

The performed analyses revealed that the oxygen precipitation in the studied crystals was significantly enhanced in the H- and L-bands. This effect, unpublished by other authors, was explained by a qualitative model of formation of crystal defects in boron-doped silicon. The presented model explains enhanced precipitation of oxygen through coincident effect of high boron concentration, high oxygen concentration, and favorable thermal history. The dependence of the equilibrium concentration of silicon interstitials on boron concentration or incorporation of boron into oxide precipitates were identified as possible mechanisms behind the enhanced oxygen precipitation.

Based on results of this work the author implemented new analytical methods for defect study and optimized crystal growth processes in ON Semiconductor CR:

- the chromium-free OISF test;
- the COP test;
- the copper decoration technique;
- the crystal growth process optimized through  $v/G$  for suppression of defect formation;
- the OISF test with pre-annealing.

The goals of the work were met.

## LITERATURA

- [1] ASTM F723-99, "Standard Practice for Conversion between Resistivity and Dopant Density for Boron-Doped, Phosphorus-Doped, and Arsenic-Doped Silicon", ASTM International, 2003.
- [2] ASTM F1188-02, "Standard Test Method for Interstitial Atomic Oxygen Content of Silicon by Infrared Absorption with Short Baseline", ASTM International, 2003.
- [3] K. H. Yang, J. Electrochem. Soc. 131 (1984) 1140.
- [4] E. Dornberger, D. Gräf, M. Suhren, U. Lambert, P. Wagner, F. Dupret, and W. von Ammon, J. Cryst. Growth, 180 (1997) 343.
- [5] G. Borionetti, D. Gambaro, M. Porrini, and V. V. Voronkov, in Semiconductor Silicon 2002, H. R. Huff, L. Fabry, and S. Kishino, editors, PV 2002-2 The Electrochemical Society Proceedings Series, Pennington, NJ (2002), p. 505.
- [6] V.V. Voronkov, R. Falster, J. Appl. Phys. 87 (2000) 4126.
- [7] V.V. Voronkov, J. Cryst. Growth 59 (1982) 625.
- [8] V.V. Voronkov, J. Cryst. Growth 59 (1982) 625.
- [9] V.V. Voronkov, R. Falster, J. Appl. Phys. 86 (1999) 5975.
- [10] V.V. Voronkov, J. Cryst. Growth 310 (2008) 1307.
- [11] V.V. Voronkov, R. Falster, J. Cryst. Growth 204 (1999) 462.
- [12] M. Suhren, D. Gräf, U. Lambert and P. Wagner, J. Electrochem. Soc. 144 (1997) 4041.
- [13] J.- M. Kim, J.- Y. Choi, H.- J. Cho, H.- W. Lee and H.- D. Yoo, Jpn. J. Appl. Phys. 40 (2001) 1370.
- [14] E. Asayama, T. Ono, M. Takeshita, M. Hourai, M. Sano, and H. Tsuya, in H.R. Huff, U. Gösele, and H. Tsuya, editors, Semiconductor Silicon 1998, PV 1998-1, The Electrochemical Society, Pennington, NJ (1998), p. 546.
- [15] T. Y. Tan, C. Y. Kung, J. Appl. Phys. 59 (1986) 917.
- [16] F. Ishikawa, T. Saishoji, K. Nakamura, and J. Tomioka, Extended Abstracts of the 58th Autumn Meeting, Japan Society of Applied Physics (1997) 243.
- [17] F. Shimura, Oxygen in Silicon, Academic Press, London (1994).
- [18] A. Borghesi, B. Pivac, A. Sassella, A. Stella, J. Appl. Phys. 77 (1995) 4169.
- [19] P. Hopfanger, P. Collareta, M. Porrini, Mater. Sci. Eng. B73 (2000) 158.
- [20] B. Borionetti, D. Gambaro, S. Santi, M. Borgini, P. Godio, S. Pizzini, Mater. Sci. Eng. B73 (2000) 218. 30
- [21] K. Sueoka, M. Akatsuka, M. Okui and H. Katahama, in H. R. Huff, U. Gösele, H. Tsuya, editors, Semiconductor Silicon 2002, PV2002–2, The Electrochemical Society, Pennington, NJ (2002), p. 540.
- [22] L. Válek, J. Šik, D. Lysáček, Enhanced oxygen precipitation during the Czochralski crystal growth, Sol. State Phenom. 131-132 (2008) 167.
- [23] L. Válek, D. Lysáček, J. Šik, OISF pattern and grown-in precipitates in heavily boron doped silicon, J. Electrochem. Soc. 154 (2007) H904.

- [24] E. Dornberger, Prediction of OSF Ring Dynamics and Grown-in Voids in Czochralski Silicon Crystals, PhD thesis, Universite Catholique de Louvain, Louvain-la-Neuve (1997).
- [25] M. Hourai, H. Nishikawa, T. Tanaka, S. Umeno, E. Asayama, T. Nomachi and G. Kelly, in H. R. Huff, U. Gösele, H. Tsuya, editors, Semiconductor Silicon 1998, PV1998-1, The Electrochemical Society, Pennington, NJ (1998), p. 453.
- [26] G. Kissinger, J. Vanhellemont, U. Lambert, D. Gräf, E. Dornberger and H. Richter, J. Electrochem. Soc. 145 (1998) 75.
- [27] N. Ono, K. Harada, J. Furukawa, K. Suzuki, M. Kida and Y. Shimanuki, in H. R. Huff, U. Gösele, H. Tsuya, editors, Semiconductor Silicon 1998, PV1998-1, , The Electrochemical Society, Pennington, NJ (1998), p. 503.
- [28] T. Sinno, H. Susanto, R.A. Brown, W. von Ammon, E. Dornberger, Appl. Phys. Lett. 75 (1999) 1544.
- [29] O. De Gryse, J. Vanhellemont, P. Clauws, O. Lebedev, J. Van Landuyt, E. Simoen, C. Claeys, Physica B 340-342 (2003) 1013.
- [30] T. Ono, E. Asayama, H. Horie, M. Hourai, K. Sueoka, H. Tsuya and G. Rozgonyi, J. Electrochem. Soc. 146 (1999) 2239.
- [31] H. Takeno, K. Aihara, Y. Hayamizu, Y. Kitawara, in H.R. Huff, U. Gösele, H. Tsuya, editors, Semiconductor Silicon 1998, PV1998-1, The Electrochemical Society, Pennington, NJ (1998), p. 1013.
- [32] D.A.P. Bula, W.E. Castro, Jr., V. Stojanoff, F.A. Ponce, S. Hahn, and W.A. Tiller, J. Cryst. Growth 85 (1987) 91.
- [33] W. Wijaranakula, J. Appl. Phys. 72 (1992) 2713.
- [34] K. Wada, Phys. Rev. B 30 (1984) 5884.
- [35] S.K. Bains, D.P. Griffiths, J.G. Wilkes, R.W. Series, G.K. Barraclough, J. Electrochem. Soc. 137 (1990) 647.
- [36] L.I. Huang, P.C. Lee, C.K. Hsieh, W.C. Shu, C.W. Lan, J. Crystal Growth 266 (2004) 132.

## CURRICULUM VITAE

### Osobní informace:

Jméno a příjmení	Lukáš Válek
Věk:	32 let
Místo narození:	Bílovec, okres Nový Jičín
Národnost:	česká
Rodinný stav:	ženatý

### Zaměstnání:

od 08/2003	ON Semiconductor Czech Republic, Rožnov pod Radhoštěm, výzkumný a vývojový pracovník
------------	--

### Vzdělání:

2007 -	doktorské studium Vysoké učení technické v Brně, obor Fyzikální a materiálové inženýrství, téma "Růstové defekty v monokrystalech Czochralského křemíku"
1998 - 2003	magisterské studium Vysoké učení technické v Brně, obor Fyzikální inženýrství, diplomová práce „Epitaxní vrstvy para-hexafenyly deponované na podložky KCl, ITO a sklo metodou Hot Wall Epitaxy“
2002	Univerzita J. Keplera, Linz, Rakousko, 6 měsíční stáž v rámci programu Erasmus, problematika přípravy epitaxních vrstev
1994 - 1998	Gymnázium Mikoláše Koperníka, Bílovec

## **ABSTRAKT**

Disertační práce se zabývá studiem defektů v monokrystalech Czochralskiho křemíku legovaných bórem. Práce studuje vznik kruhových obrazců vrstevných chyb pozorovaných na povrchu křemíkových desek po oxidaci. Hlavním cílem práce je objasnit mechanismy vzniku pozorovaného rozložení vrstevných chyb na studovaných deskách a vyvinout metody pro řízení tohoto jevu.

Na základě experimentálních analýz a rozborů obecných mechanismů vzniku defektů jsou objasňovány vazby mezi vznikem defektů různého typu. Tyto jsou pak diskutovány v souvislosti s parametry krystalu i procesu jeho růstu. Takto sestavený model je využit pro vývoj procesu růstu krystalů, kterým je potlačen nadměrný vznik defektů ve studovaných deskách. Za účelem studia defektů jsou zaváděny a vyvíjeny nové analytické metody.

Disertační práce byla vytvořena za podpory ON Semiconductor Czech Republic, Rožnov pod Radhoštěm.

## **ABSTRACT**

The doctoral thesis deals with analyses of defects in single crystals of Czochralski silicon doped with boron. Mechanisms of formation of circular patterns of oxidation induced stacking faults are studied. The main goal of the work is to explain the mechanisms of formation of the observed defect patterns and to develop methods for control of this phenomenon.

Mechanisms of defect formation in silicon are analyzed and the material is experimentally studied in order to explain relations between formation of defects of various kinds and to link these processes to parameters of the crystal and its growth. A qualitative model capturing all these relations is built and utilized to develop an optimized crystal growth process for suppression of excessive formation of the oxidation induced stacking faults. Novel methods are developed and implemented to support effective analyses of crystal defects.

This doctoral thesis was written with the support of ON Semiconductor Czech Republic, Rožnov pod Radhoštěm.